A Tale of two Higgs: Search for pair production of Higgs bosons in the $b\bar{b}b\bar{b}$ final state using proton–proton collisions at $\sqrt{s} = 13$ TeV with the ATLAS detector

A DISSERTATION PRESENTED
BY
BAOJIA TONG
TO
THE DEPARTMENT OF PHYSICS

IN PARTIAL FULFILLMENT OF THE REQUIREMENTS
FOR THE DEGREE OF
DOCTOR OF PHILOSOPHY
IN THE SUBJECT OF
PHYSICS

HARVARD UNIVERSITY
CAMBRIDGE, MASSACHUSETTS
MAY 2018

Thesis advisor: Professor Melissa Franklin Baojia Tong

A Tale of two Higgs: Search for pair production of Higgs bosons in the $b\bar{b}b\bar{b}$ final state using proton–proton collisions at $\sqrt{s} = 13$ TeV with the ATLAS detector

Abstract

This thesis presents a search for Higgs boson pair production, with the $b\bar{b}b\bar{b}$ final state. This analysis uses the full 2015 and 2016 data collected collected by the ATLAS Collaboration at $\sqrt{s} = 13$ TeV, corresponding to 3.2 ± 0.2 fb^{-1} of 2015 and 32.9 ± 1.1 fb^{-1} of 2016 pp collision data. Improvements with respect to the previous analysis come from the increased dataset, detailed background estimation and addtional signal regions. Search sensitivity is specially enhanced for the resonance signals between 2500 GeVand 3000 GeV. The data is found to be compatible with the Standard model, and no signs of new physics have been observed. The results are interpreted in the context of the bulk Randall-Sundrum warped extra dimension model with a Kaluza-Klein graviton decaying to hh, with the coupling $k/\bar{M}_{\mathrm{Pl}} = 1.0$ or 2.0. The results are also interpreted with the Type 2 two-Higgs doublet model (2HDM) where the neutral heavy CP-even H scalar decays to hh.

Contents

Listing of figures

Listing of tables

Everything is meaningless.
Even the sentence above.

Acknowledgments

Thanks to everyone working at CERN. CERN is a truely unique and special place. I love how the streets are named by physicists. Without the support from the IT department, I could not log into lxplus, check the twikis and finish my work. CERN user's office also made traveling to Europe a much nicer and easier experience for me.

Thanks to everyone working on the Large Hadron Collider. Without a fully functional accerator, there would have been no data for me to study. The LHC performed outstandingly since 2015, and all the valuable data is produced from it.

Thanks to everyone the ATLAS collaboration, who has supported this remarkable program and has contributed to every bit of the result in my thesis. Sir Issac Newton said he was standing on the gaint's showlders to see far and deep into the nature. Similarly. I am standing on the ATLAS(member)'s showlders–it's eight stories high so I hope ATLAS doesn't shrug. Without the excellent work on detector design, commisioning, operational works, reconstruction, data processing, performance studies and recommendations, software support, computing support, and analysis discussions and guidance, I could not have completed this thesis. I truely and sincerely thank all

ATLAS members for their contributions.

0

Introduction

Why do we look for $hh \to 4b$?

There are two types of analysis in particle physics. The first one is measurement, which yeilds a observable with an uncertainty. This could either imrpove our current knowledge, or show some inconsistency. The other type is search, which generally assumes some new physics model and try to justfy in data wether the new model is justified in some observables. A successful search turns the subject into a measurement, yet a null search result will set a new limit for a given physics model.

After Run 1 of the LHC, with the existence of the Higgs now firmly established, the focus shifted to searches for physics beyond the Standard Model. In particular, searches for high mass resonances

benefit from the LHC's increase to $\sqrt{s} = 13$ TeV in Run 2. The cross section for a generic gluon-initiated resonance with a mass of 2 TeV increases tenfold in Run 2, making searches for high mass resonances a high priority. The newly discovered Higgs can be used as a tool in these searches. After the discovery, the Higgs boson provides a large swath of unmeasured phase space where new physics could be discovered. Higgs pair production in the Standard Model has a low cross section that requires large datasets (on the order of the LHC's lifetime) for full measurement. However, new physics can modify this cross section, especially through new resonances which decay to two Higgs bosons. Such high mass resonances also produce difficult to recognize final state topologies due to the merging of decay products from high momentum Higgs bosons. A search for Higgs pair production in the $HH \to b\bar{b}b\bar{b}$ final state was performed with 3.2fb^{-1} collected with ATLAS at $\sqrt{s} = 13$ TeV in 2015. The results are presented in this dissertation with a focus on a dedicated signal region for boosted final states. This signal region uses new techniques for recognizing jet substructure and b-tagging to the improve signal acceptance of high mass resonances.

The discovery of the Standard Model (SM) Higgs boson (h)[?,?] at the Large Hadron Collider (LHC) motivates searches for new physics using the Higgs boson as a probe. In particular, many models predict cross sections for Higgs boson pair production that are significantly greater than the SM prediction. Resonant Higgs boson pair production is predicted by models such as the bulk Randall–Sundrum model[4,5], which features spin-2 Kaluza–Klein gravitons, G^*_{KK}, that subsequently decay to a pair of Higgs bosons. Extensions of the Higgs sector, such as two-Higgs-doublet models[6,7], propose the existence of a heavy spin-0 scalar that can decay into $h$pairs. Enhanced non-resonant Higgs boson pair production is predicted by other models, for example those featuring light coloured scalars[8] or direct $t\bar{t}hh$ vertices[9,10].

Previous searches for Higgs boson pair production have all yielded null results. In the $b\bar{b}b\bar{b}$channel, ATLAS searched for both non-resonant and resonant production in the mass range of 400–3000 GeV using 3.2 fb^{-1} of 13 TeV data[11] collected during 2015. CMS searched for the production of resonances

with masses of 750–3000 GeV[7] using 13 TeV data and with masses 270–1100 GeV with 8 TeV data[8]. Using 8 TeV data, ATLAS has examined the $b\bar{b}b\bar{b}$[12], $b\bar{b}\gamma\gamma$[13], $b\bar{b}\tau^+\tau^-$ and $W^+W^-\gamma\gamma$ channels, all of which were combined in Ref.[8]. CMS has performed searches using 13 TeV data for the $b\bar{b}\tau^+\tau^-$[9] and $bb\ell\nu\ell\nu$[10] final states, and used 8 TeV data to search for $b\bar{b}\gamma\gamma$[11] in addition to a search in multilepton and multilepton+photons final states[8].

The analyses presented in this paper exploit the dominant $h \to b\bar{b}$ decay mode to search for Higgs boson pair production in both resonant and non-resonant production. Two analyses are presented, which are complementary in their acceptance, each employing a unique technique to reconstruct the Higgs boson. The "resolved" analysis is used for hh systems in which the Higgs bosons have Lorentz boosts low enough that four b-jets can be reconstructed. The "boosted" analysis is used for those hh systems in which the Higgs bosons have higher Lorentz boosts, which prevents the Higgs boson decay products from being resolved in the detector as separate b-jets. Instead, each Higgs boson candidate consists of a single large-radius jet, and b-decays are identified using smaller-radius jets built from charged-particle tracks.

Both analyses were re-optimized with respect to the former ATLAS publication[11]; an improved algorithm to pair b-jets to Higgs boson candidates is used in the resolved analysis, and in the boosted analysis an additional signal-enriched sample is utilized. The dataset comprises the 2015 and 2016 data, corresponding to 27.5 fb^{-1} for the resolved analysis and 36.1 fb^{-1} for the boosted analysis, with the difference due to the trigger selections used. The results are obtained using the resolved analysis for a resonance mass between 260 and 1400 GeV, and the boosted analysis between 800 GeV and 3000 GeV. The main background is multijet production, which is estimated from data; the subleading background is $t\bar{t}$, which is estimated using both data and simulations. The two analyses employ orthogonal selections, and a statistical combination is performed in the mass range where they overlap. The final discriminants are the four-jet and dijet mass distributions in the resolved and boosted analyses, respectively. Searches are performed for the following benchmark signals: a spin-2

graviton decaying into Higgs bosons, a scalar resonance decaying into a Higgs boson pair, and SM non-resonant Higgs boson pair production.

This dissertation begins by discussing the status of di-Higgs. Chapter 1 gives an overview of double Higgs production in the Standard Model and beyond. Chapter 2 and 3 present details regarding the Large Hadron Collider and the ATLAS experiment. Chapter 4 provides an overview of object reconstruction in ATLAS, with a focus on Muon Segment Seeding. A brief interlude in Chapter 5 on the ATLAS Muon Data Quality, as this has been a focus of my graduate work.

The rest of the dissertation presents a search for Higgs pair production in the $HH \to b\bar{b}b\bar{b}$ channel. Chapter 6 presents an overview of physics object selection, where the Higgs pairs are the result of the decay of a heavy resonance. Chapter 7 discusses the background estimation techinics in detail, followed by Chapter 8, Systematics. Chapter 9 presents the results, and Chapter 10 shows the limits between the boosted regime and the resolved regime, which is sensitive to lower mass resonances and non-resonant Higgs pair production. Finally, the work is summaried a conclusion and brief outlook of future Higgs physics with ATLAS.

Knowledge knows no bounds.

Creator

1

Theory and Motivation

1.1 The Standard Model and the Higgs Boson

The Standard Model(SM) [1,14,15,16] is a quantum field theory describing the interactions of fundamental particles. The partciles are shown in Figure 1.1. So far, the SM predictions agree extremely well with experimental observations.

In the SM, the Higgs mechanism introduces a complex scalar Higgs field, φ, with nonzero vacuum expectation values. The scalar Higgs potential is $V(\varphi) = -v^2\lambda_v\varphi^\dagger\varphi + \lambda_v(\varphi^\dagger\varphi)^2$. Through spontaneous symmetry breaking, $W^\pm$ and Z bosons acquire their masses. This process also predicts an extra scalar, the Higgs boson. The SM Lagrangian containing Higgs couplings, $\mathcal{L}_{\text{Higgs}}$, is shown

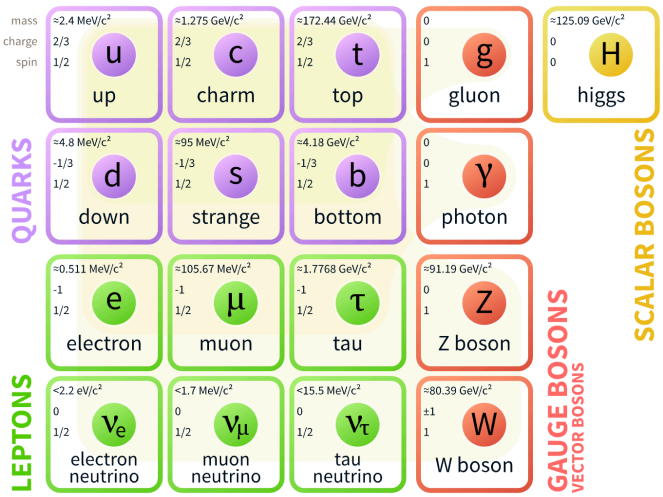

Figure 1.1: Fermions and bosons of the Standard Model and their properties [1], where all the values are measured experimentally.

in Eq 1.1.

$$\mathcal{L}_{\text{Higgs}} = -\lambda_{h\bar{f}f} h\bar{f}f + \delta_V V_\mu V^\mu \left(\lambda_{\text{hVV}} h + \lambda_{\text{hhVV}} h^2\right) + \lambda_{\text{hh}} h^2 + \lambda_{\text{hhh}} h^3 + \lambda_{\text{hhhh}} h^4 \qquad (1.1)$$

where

- $v \sim 246$ GeV, is the non-zero expectation value of the Higgs field;
- $m_{\text{h}} = \sqrt{2\lambda_v} v \sim 125$ GeV, is the Higgs mass; this is discovered in 2012 [17,18];
- λ_v, coefficient for the quartic potential term, is constrained from Higgs mass, to be ~ -0.13;
- $V = W^\pm$ or Z, $\delta_W = 1$, $\delta_Z = \frac{1}{2}$;
- $\lambda_{h\bar{f}f} = \frac{m_{\text{f}}}{v}$, is the Higgs to fermion coupling; m_{f} is the mass of the fermion;
- $\lambda_{\text{hVV}} = \frac{2m_{\text{V}}^2}{v}$, is the Higgs to boson coupling; m_{V} is the mass of the boson;
- $\lambda_{\text{hhVV}} = \frac{m_{\text{V}}^2}{v^2}$, is the Higgs-Higgs to boson-boson coupling;
- $\lambda_{\text{hh}} = \frac{m_{\text{h}}^2}{2}$, is the Higgs mass term;

- $\lambda_{hhh} = \frac{m_h^2}{2v} = \lambda_v v$, or λ_{hhh}, is the Higgs self-coupling;
- $\lambda_{hhh} = \frac{m_h^2}{8v^2}$, is the Higgs quartic-coupling.

What's particularly interesting and has not been measured experimentally in Eq 1.1 is λ_{hhh}. SM predicts $\lambda_{hhh} = \frac{m_h^2}{2v}$, which is referred as λ_{SM} in this thesis. This term directly probes the Higgs potential. Also, $\lambda_{hhh} h^3$ term shows one way for double Higgs production within the SM. Double Higgs production is also known as di-Higgs or Higgs pair production.

1.2 Standard Model di-Higgs production

There are two main production diagrams of di-Higgs at the LHC, shown in Figure 1.2. In the gluon-gluon fusion process, di-Higgs are produced through a box or a triangle loop. Only the triangle loop 1.2b probes the λ_{hhh}. In the triangle diagram, the middle Higgs boson acts as a propagator (off-shell), and the two Higgs boson in the final state are on-shell. An on-shell middle Higgs, with two off-shell Higgs bosons in the final state, is strongly disfavored[1]. The box and triangle diagrams interfere destructively, which makes the overall production rate smaller than what would be expected in the absence of a λ_{hhh} term.

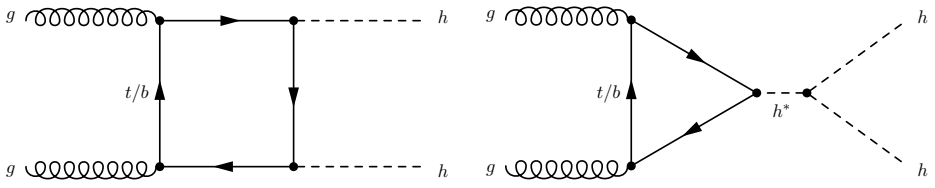

(a) Box diagram **(b)** Triangle diagram

Figure 1.2: Leading order Feynman diagrams contributing to di-Higgs production via gluon-gluon fusion, through the Higgs-fermion Yukawa interactions 1.2a and the Higgs boson self-coupling 1.2b. Only Figure 1.2b probes λ_{hhh}.

Many other different production modes of di-Higgs exist, but gluon-gluon fusion is the dominant one. Figure 1.3[19] compares the cross sections of gluon-gluon fusion, Vector Boson Fusion (VBF), and top-pair, $W^{\pm}$, Z and single-top associated di-Higgs production.

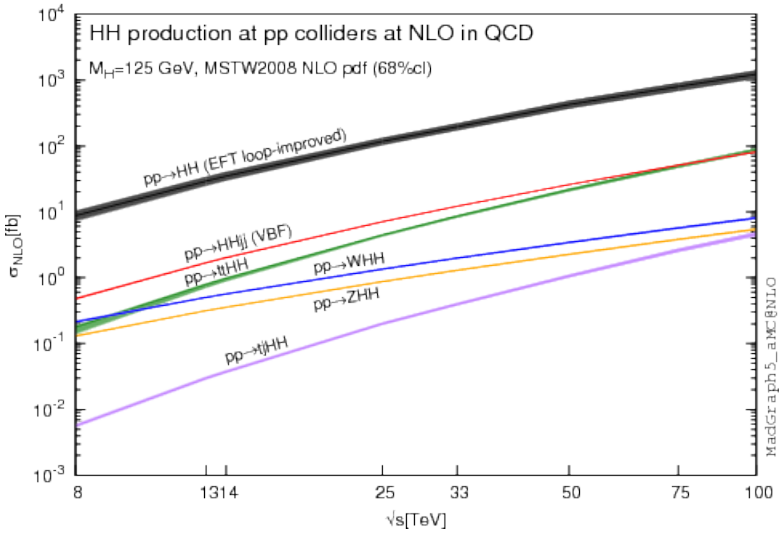

Figure 1.3: Total cross sections (y-axis) at the NLO in QCD for the six largest di-Higgs production channels at p-p colliders at different energy (x-axis). The thickness of the lines corresponds to the scale and PDF uncertainties added linearly. H refers to the SM Higgs.

For p-p collisions at $\sqrt{s} = 13$ TeV, the total cross section for SM gluon fusion di-Higgs production[20], at the Next to Next Leading Order (NNLO) with top quark mass effects, is $33.49^{+4.3\%}_{-6.0\%} \pm 2.1\% \pm 2.3\%$ fb. The cross section for the next dominant production, VBF, is $1.62^{+2.3\%}_{-2.7\%} \pm 2.3\%$ fb. The estimated cross section for triple-Higgs production is $0.06332^{+16.1\%}_{-14.1\%} \pm 3.4\%$ fb, which is negligible with current dataset. The uncertainties are Scale uncertainty, PDF uncertainty and α_s uncertainty. This means inside 2015 and 2016 $\sqrt{s} = 13$ TeVATLAS 36 fb^{-1}data , there are only around one thousand SM di-Higgs events.

1.3 Beyond the Standard Model physics di-Higgs production

The SM works extremely well, yet the Higgs boson mass at 125 GeV requires extreme fine-tuning for radiative corrections. The presence of new physics at the TeV scale would help solve the natrualness problem.

BSM physics could significantly enhance the production of di-Higgs at the LHC. This is separated into two categories: non-resonant and resonant productions. The non-resonant production generally refers to modifications of the Higgs couplings, either the Higgs self-coupling or the Higgs-top couplings. Resonant production refers to a particle with invariant mass greater than twice the Higgs mass decays directly into two Higgs bosons. The difference also comes from the distribution of the di-Higgs invariant mass at the truth level. In the non-resonant case, the distribution has no clear peak, whereas in the resonant case, the invariant mass distribution usually forms a peak with model dependent width.

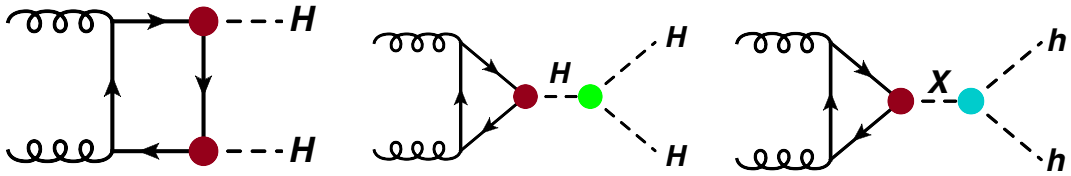

(a) H-fermion vertices variations **(b)** Higgs self-coupling variations **(c)** an intermidiate resonance, X

Figure 1.4: BSM Higgs boson pair production: non-resonant production proceeds through changes in the SM Higgs couplings in 1.4a and 1.4b, resonant production proceeds through 1.4c an intermediate resonance, X. H and h both refers to the SM Higgs.

1.3.1 BSM non-resonant di-Higgs

Enhanced non-resonant Higgs boson pair production is predicted by many models. Models featuring direct $t\bar{t}hh$ vertices[9,10] or new light colored scalars[8] could change vertices shown as the red

dots in Figure 1.4. A direct modification of Higgs self-coupling term in Eq 1.1 to λhhh, where λ is different from λ_{sm}, is also possible. This is shown as the green dot in Figure 1.4b.

The non-resonant di-Higgs enhancement is usually described by $\frac{\lambda}{\lambda_{SM}}$, which is the cross section ratio between λ and λ_{SM}. From the SM electroweak measurements, the self coupling term could be constrained to $-14 \leq \frac{\lambda}{\lambda_{SM}} \leq 17.4$ [21]. Variations of λ have a non-trivial effect on di-Higgs production cross section, shown in Figure 1.5 [19]. In the regime of relatively high trilinear coupling, the observation will be an excess of di-Higgs events with respect to the expected background. A simple limit can be set in this case.

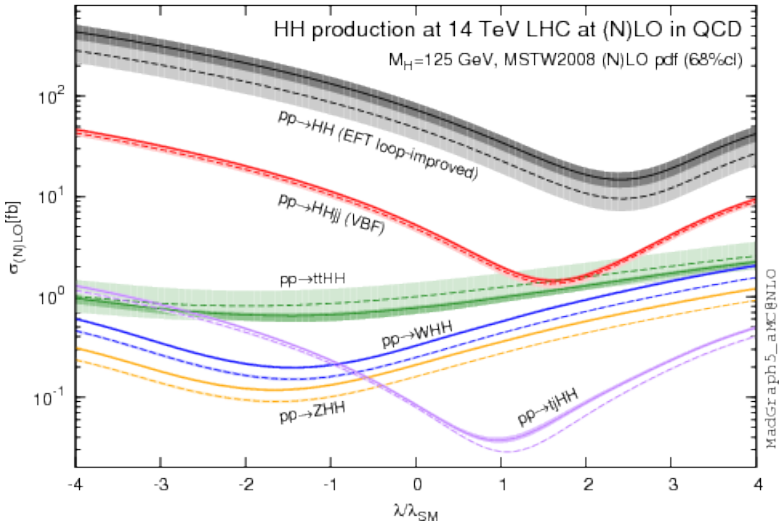

Figure 1.5: Total cross sections (y-axis) at the LO and NLO in QCD for di-Higgs production channels, at the $\sqrt{s} = 14$ TeV LHC as a function of the self-interaction coupling λ (x-axis) . The dashed (solid) lines and light- (dark-) color bands correspond to the LO (NLO) results and to the scale and PDF uncertainties added linearly. The SM values of the cross sections are obtained at $\frac{\lambda}{\lambda_{SM}} = 1$. H refers to the SM Higgs.

1.3.2 BSM resonant di-Higgs

Resonant Higgs boson pair production is also predicted by many models. Extensions of the Higgs sector, such as two-Higgs-doublet models(2HDM) [6,7], propose the existence of a heavy spin-0 scalar

H that can decay into di-Higgs. The bulk Randall-Sundrum model [4,5], which features spin-2 Kaluza-Klein gravitons, G^*_{KK}, could also subsequently decay to pairs of Higgs bosons. These proposed heavy particles, heavy CP-even scalar H and G^*_{KK}, are represented as X in Figure 1.4c.

The 2HDM is a a simple extension of the SM which can exhibit large resonance effects [20]. The 2HDM has 5 physical Higgs bosons: h (light scalar Higgs), H (heavy scalar Higgs), A (heavy pesudoscalar Higgs), and $H^{\pm}$ (two charged Higgs). The 2HDM can introduce tree level favor changing neutral currents. To avoid this, models impose discrete symmetries in which the charged fermions only couple to one of the Higgs doublets. One version is type II 2HDM, in which all positively charged quarks couple to one doublet and the negatively charged quarks and leptons couple to the other. The type II model is the Minimal Supersymmetric Standard Model(MSSM)'s Higgs sector.

Resonant di-Higgs production in 2HDM models can proceed through decays of the heavy CP-even Higgs $H \rightarrow hh$. The branching ratio for $H \rightarrow hh$ depends on the model type as well as the values of $\tan\beta$ and $\cos(\beta - \alpha)$. $\tan\beta = \frac{v_{\text{doublet2}}}{v_{\text{SM}}}$ is the ratio of the vacuum expectation values of the two Higgs doublets. α is the mixing angle between the heavy H and light h fields. The limit where $\cos(\beta - \alpha) = 0$ is called the alignment limit, and in this limit the light Higgs h has the same couplings as a SM Higgs. Near the alignment limit there is some unprobed phase space depending on the exact models and values of $\tan\beta$ being considered, and they are particulary interesting to be searched for at the LHC.

The Randall-Sundrum model proposes a five-dimensional warped spacetime that contains two manifolds: one where the force of gravity is very strong and a second manifold at the TeVscale corresponding to the known SM sector. The experimental consequence of this theory is a series of widely mass-spaced Kaluza-Klein graviton resonances, G^*_{KK}. In theories where the fermions are localized to the SM brane, production of gravitons from fermion pairs is suppressed and the primary

mode of production of $G^*_{KK}$is gluon fusion. These gravitons have a substantial branching fraction to di-Higgs, ranging from 6.43% for gravitons with a mass of 500 GeVto 7.66% at 3 TeV. Randall-Sundrum models have two free parameters - the mass of the graviton and $c = k/\bar{M}_{pl}$, where $\bar{M}_{pl}$ is the reduced Planck mass and k is the curvature parameter. The width of the graviton increases with both mass and c.

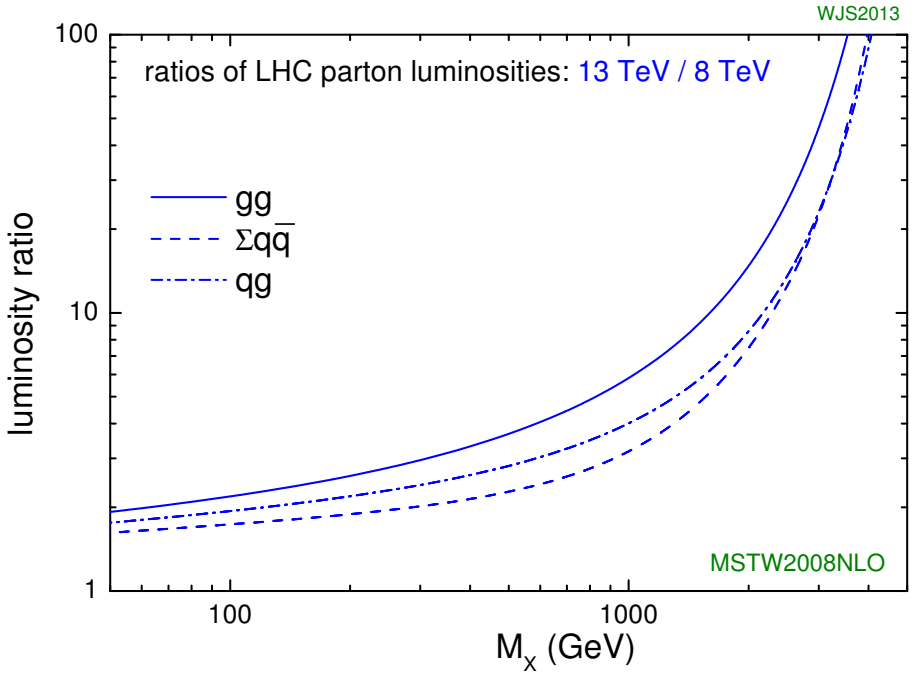

Figure 1.6: Parton luminosity ratios as a function of resonance mass M_X for 13/8 TeV [2]. For a 2 TeV X, the lumniosity ratio is almost 10.

In model dependent searches, based on fixed assumptions of the resonance particles' branching ratio, other search channels like resonance VV or $t\bar{t}$ are more sensitive compared to di-Higgs [22]. In order to constrain more BSM physics phase space, di-Higgs search restuls need to be interpreted in different baseline models, covering both narrow and wide resonances.

Generally, it is easy theoretically for new heavy resonance particles to interact with the SM through the Higgs as a portal, resulting in resonance di-Higgs production. With the increased center of mass collision energy from 8 TeV to 13 TeV, the production cross section through gluon-gluon fusion for heavy particles above TeV grows in LHC Run 2, as shown in Figure 1.6. Therefore, it is particularly important to focus on resonant searches above TeV region.

1.4 Di-Higgs decay and LHC previous search results

Di-Higgs decay is a combination of single Higgs decays. The coupling terms to fermions and bosons are shown in Eq 1.1. The branching ratio of the di-Higgs final state is shown in Figure 1.7.

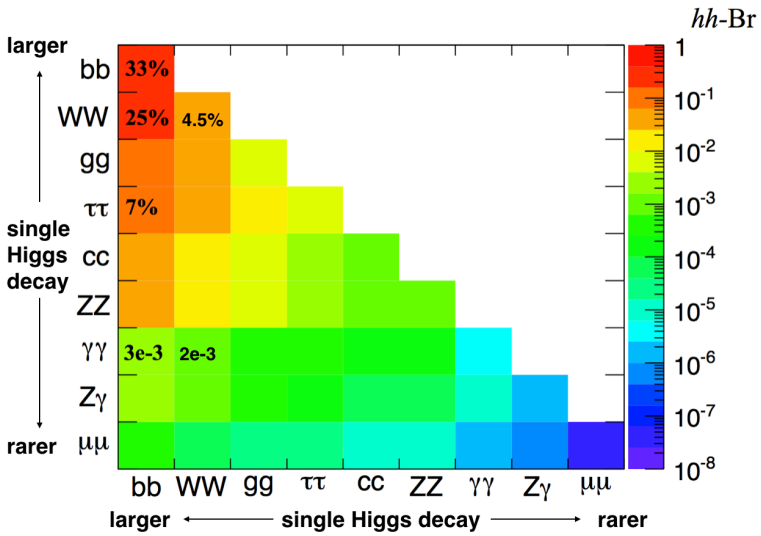

Figure 1.7: Summary of di-Higgs final states and their ratios. Top left, $b\bar{b}b\bar{b}$, has the largest branching ratio.

Previous searches for Higgs boson pair production have all yielded null results. Using 8 TeV data, ATLAS has examined the $b\bar{b}b\bar{b}$ [12], $b\bar{b}\gamma\gamma$ [13], $b\bar{b}\tau^+\tau^-$ and $W^+W^-\gamma\gamma$ channels, all of which were combined [23]. The resonant search combination result is shown in Figure 1.8. The best non-resonant $\sigma(pp \to hh)$ cross section limit in Run 1 is the ATLAS combination, at 0.69 pb. This crossponds to

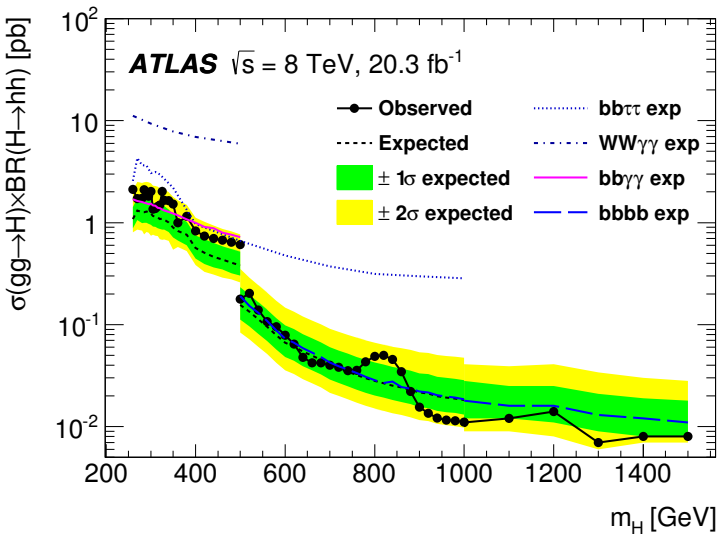

Figure 1.8: The observed and expected 95% CL upper limits of $\sigma(gg \to H) \times BR(H \to hh)$ at $\sqrt{s} = 8$ TeV as functions of the heavy Higgs boson mass m_H, combining resonant searches in Higgs boson pair to $b\bar{b}\tau^+\tau^-$, $W^+W^-\gamma\gamma$, $b\bar{b}\gamma\gamma$, and $b\bar{b}b\bar{b}$ final states. The expected limits from individual searches are also shown. The green and yellow bands represent $\pm 1\sigma$ and $\pm 2\sigma$ uncertainty ranges of the expected combined limits. The improvement above $m_H = 500$ GeV reflects the sensitivity of the $b\bar{b}b\bar{b}$ analysis. The results beyond 1 TeV are only from the $b\bar{b}b\bar{b}$ final state alone.

$\frac{\lambda}{\lambda_{SM}} < 70$. Different di-Higgs search challenges and perspectives are summarized below:

- $b\bar{b}b\bar{b}$: Trigger limits the low mass resonance searches, but for high mass resonances above 500 GeV, the branching ratio of this channel provides a decisive advantage. Great for non-resonant searches.
- $b\bar{b}W^+W^-$: Despite the second largest branching ratio, large background from $t\bar{t}$ limits this search sensitivity.
- $b\bar{b}\gamma\gamma$: Benefit from a good double photon trigger efficiency, a good photon reconstruction efficiency and a low SM background. Most sensitive at low mass $m_X \leq 350$ GeV. At higher masses, the smaller branching ratio and the merging of photons hurt the search sensitivity. Great for non-resonant searches.
- $b\bar{b}\tau^+\tau^-$: An intermediate choice between $b\bar{b}b\bar{b}$ and $b\bar{b}\gamma\gamma$ for resonance searches. Yet this channel contributes to the non-resonant result significantly.
- $W^+W^-\gamma\gamma$: Suffers from much lower branching ratio and lower reconstruction efficiency of the W^+W^- compared to $b\bar{b}$.

- $W^+W^-\tau\tau$, $W^+W^-W^+W^-$, $b\bar{b}ZZ$: There are no search results on these channels yet. But because of the relatively large branching ratio, it is likely that they would be explored in the future.

In summary, di-Higgs has a small production rate in the SM, but could be significantly enhanced in BSM scenarios. In particular, a heavy resonance spin-0 or spin 2 particle could decay into Higgs boson pair directly. The search sensitivity for massive resonances increases as the center of mass energy of the collision increases. For resonance signals above 1 TeV decaying into di-Higgs, $b\bar{b}b\bar{b}$ channel has the best discovery potential in Run 2. Therefore, searching for TeV scale resonance production of di-Higgs $\rightarrow b\bar{b}b\bar{b}$ is the goal of thesis.

Pain teaches lessons no scholar can.

2

LHC and ATLAS

The Large Hadron Collider (LHC) is a proton-proton collider at the European Organization for Nuclear Research (CERN) laboratory in Geneva, Switzerland[24]. ATLAS (A Toroidal LHC ApparatuS), CMS (the Compact Muon Solenoid), ALICE (A Large Ion Collider Experiment), and LHC*b*[25,26,27,28] are the four main experiments. They are located at the Interaction points(IPs) of the accelerator. Figure 2.1 shows a schematic of the LHC ring and its experiments.

2.1 The Large Hadron Collider

Protons accelerated in the LHC are from a red bottle of hydrogen gas. The whole acceleration takes around 25 minutes:

- An electric field strips the electrons from the hydrogen to create protons;

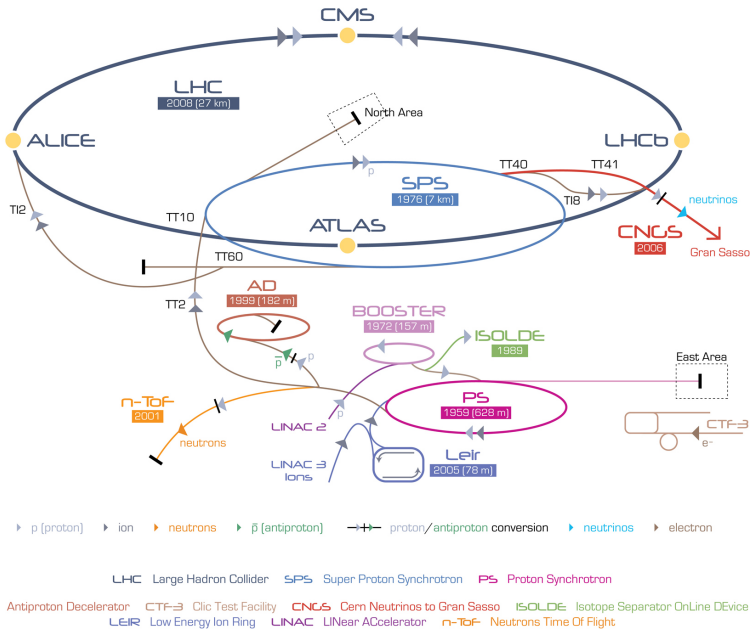

Figure 2.1: A schematic view of the LHC ring[3]. LINAC2, Booster, PS, SPS, and LHC accelerate the protons in order. Four main experiments are located at interaction points along the ring. ATLAS and CMS are general purpose experiments, while ALICE focuses on heavy ion collisions and LHCb is dedicated to B physics.

- A linear particle accelerator, Linac 2, accelerates the protons to 50 MeV;
- The Proton Synchrotron Booster (PSB) accelerates the protons to 1.4 GeV;
- The Proton Synchrotron (PS) accelerates the protons to 25 GeV;
- The Super Proton Synchrotron (SPS) accelerates the protons to 450 GeV; it sends the protons in bunch trains;
- The 16.7 kilometers LHC accelerates the protons in a series of Radio Frequency cavities to the final TeV energies. The LHC uses 1232 Niobium Titanium magnetic dipole for steering the protons. They are cooled by superfluid helium to 1.9 Kelvin, and can generate 8.33 Tesla magnetic field.

In proton-proton collisions, the rate of a certain physics process $R_{\text{phy}} = L\sigma$, where $L\,(m^{-2}s^{-1})$ is the instantaneous luminosity, and $\sigma\,(m^2)$ the cross section of physics process (like di-Higgs' σ 1.2).

For a Gaussian beam profile, the instantaneous luminosity is defined in Eq2.1 [3]:

$$L = \frac{n_b N_b^2 f_{\text{rev}} \gamma_r}{4\pi \varepsilon_n \beta^*} F \tag{2.1}$$

In the above Eq2.1:

- n_b is the number of bunches per beam; n_b cannot be too large due to potential beam loss damages on the accelerator and detector;
- N_b is the number of protons per bunch;
- f_{rev} is the proton revolution frequency;
- γ_r is the relativistic Lorentz factor for the protons;
- ε_n is the average beam spread length in the transverse plane;
- β^* is the beam spread in the longitudinal direction; affected by focusing magnets;
- F is a reduction factor for the angle beams are colliding; smaller crossing angles could cause larger spread in the longitudinal direction.

The instantaneous luminosity can also be written as the ratio of the rate of inelastic collisions to the inelastic cross section σ_{inel} [29]:

$$L = \frac{R_{\text{inel}}}{\sigma_{\text{inel}}} = \frac{\mu n_b f_{\text{rev}}}{\sigma_{\text{inel}}} \tag{2.2}$$

where, μ is the number of interactions per bunch crossing. At each bunch crossing, multiple proton-proton collide, and the collisions without the highest center of mass energy are called "pileup" interactions. The target peak instantaneous luminosity for both the ATLAS and CMS experiments is $L = 10^{34}\ \text{cm}^{-2}\text{s}^{-1}$ [24], which is already exceeded in 2016. This is partly due to the rising number of "pileup" interactions. The main parameters of the LHC beam and performance are shown in Table 2.1.

Parameter [unit]	Nominal design value	2015 Operating value	2016 Operating value
Beam Energy [TeV]	7	6.5	6.5
Peak L [10^{34}cm^2 s^{-1}]	1	0.5	1.25
Bunch spacing [ns]	25	25	25
f_{rev} [kHz]	11245	11245	11245
n_b [10^{11} p/bunch]	1.15	1.15	1.12
N_b [bunch]	2808	1825	2220
ε_n [mm mrad]	3.5	3.5	2
β^* [cm]	55	80-40	40
F	0.84	0.84	0.59
$\langle\mu\rangle$	19	13	41

Table 2.1: LHC nominal [24] and operational parameters in 2015 [30] and 2016 [31].

2.2 A Toroidal LHC ApparatuS

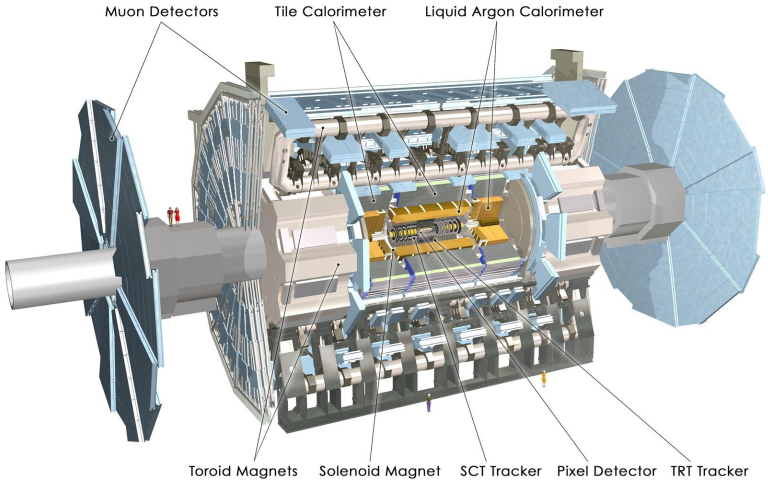

Figure 2.2: A detailed computer-generated image of the ATLAS detector and it's systems.

The ATLAS experiment [32] at the LHC is a general-purpose particle detector with a near 4π coverage in solid angle and a forward-backward symmetric cylindrical geometry. The ATLAS detector (Figure 2.2) consists of an inner tracking detector (ID) surrounded by a 2.3 m diameter thin su-

perconducting solenoid providing a 2T axial magnetic field, electromagnetic (EM) and hadronic calorimeters, and a muon spectrometer (MS). Three extra air-core toroid magnets generate the magnetic field in the MS.

2.2.1 Coordinate System

ATLAS uses a right-handed coordinate system with its origin at the nominal IP in the center of the detector and the z-axis along the beam pipe. The x-axis points from the IP to the center of the LHC ring, the y-axis points towards the sky, and the z-axis points straight(like bridges) towards the Geneva airport(A side), back from the Charlie pub in France(C side). Cylindrical coordinates (r, ϕ) are used in the transverse plane, ϕ being the azimuthal angle around the z-axis. The pseudorapidity is defined in terms of the polar angle ϑ as $\eta = -\ln\tan(\vartheta/2)$. It is the massless approximation of rapidity, the angle parameterizing special relativity's boosts. Most hadron productions are roughly constant in η, and for two massless particles travelling in different directions, their difference in $\Delta\eta$ is invariant. Therefore, angular distance is measured in units of $\Delta R = \sqrt{(\Delta\eta)^2 + (\Delta\phi)^2}$.

The region with $\eta \sim 0$ is called "central", consisting of the "barrel" elements, surrounding the beam line cylindrically. At high $|\eta| > 2.5$, the region is refered to as "forward", where "endcap" detector elements are arranged as disks perpendicular to the beam line.

2.2.2 Inner Detector

The ID covers the pseudorapidity range $|\eta| < 2.5$. It consists of three parts: silicon pixel (PIXEL), silicon microstrip (SCT), and straw-tube transition-radiation tracking (TRT) detectors. An additional pixel detector layer (IBL) [33], inserted at a mean radius of 3.3 cm, is used in the Run-2 data-taking and improves the identification of b-jets[34]. A 10 GeV charged particle in the barrel region expect $1 + 3$ IBL-Pixel hits, 8 SCT hits and 36 TRT hits.

ID is designed to provide charged particle momentum measurement with $\sigma_{p_T}/p_T \sim 0.05\% p_T \oplus 1\%$ and vertex reconstruction. Because of this, each detector proves measurement accuracies of the order 10μm in R-ϕ and 100μm in z. Figure 2.3a [35] shows the R-z distribution of the material for a quadrant of the barrel region PIXEL and SCT. The intensity of a particle beam decreases exponentially in radiation length. $I(x) = I_0 e^{-x/X_0}$, where I is the intensity, x is the distance traveled, and X_0 is the radiation length. Figure 2.3b shows the distribution of hadronic-interaction vertex candidates in $|\eta| < 2.4$ and $|z| < 400$ mm for 13 TeV data.

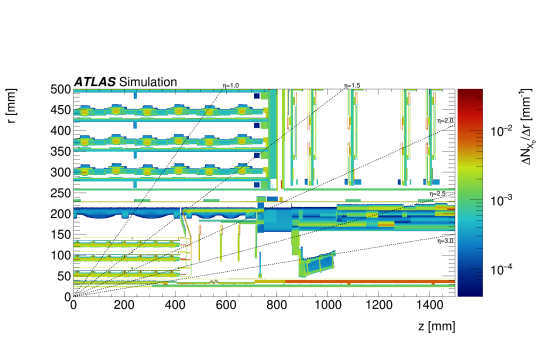

(a) The R-z distribution of material's differential number of radiation lengths, $\frac{\Delta N_{X_0}}{\Delta r}$

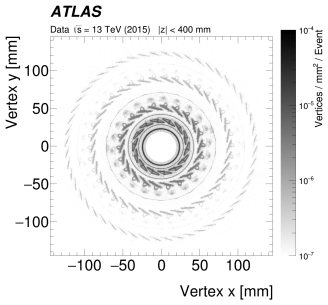

(b) Distribution of hadronic-interaction vertex candidates

Figure 2.3: Gemoetry of IBL, PIXEL and SCT detectors in Run2.

2.2.3 Calorimeter

Lead/liquid-argon (LAr) finely segmented sampling calorimeters provide EM energy measurements. A steel/scintillator-tile hadronic calorimeter (HCal) covers the central pseudorapidity range ($|\eta| < 1.7$). The endcap and forward regions are instrumented with copper/tungsten and LAr calorimeters for both the EM and hadronic energy measurements up to $|\eta| = 4.9$. The calorimeters also provide basic EM/Hadronic trigger information, with fast analogue summing in coarse granularity.

EM calorimeter (ECal) is designed to have $>$ 22 radiation lengths in the barrel and $>$ 24 in the endcap. It provides EM measurement with $\sigma_E/E = 10\%/\sqrt{E} \oplus 0.7\%$. The hadronic calorimeter (HCal) has approximately 9.7 interaction length in the barrel and 10 in the endcap. HCal provides hadronic measurement with $\sigma_E/E = 50\%/\sqrt{E} \oplus 3\%$ in the Barrel and Endcap regions, and $\sigma_E/E = 100\%/\sqrt{E} \oplus 10\%$ in the forward region.

2.2.4 MuonSpectrometer

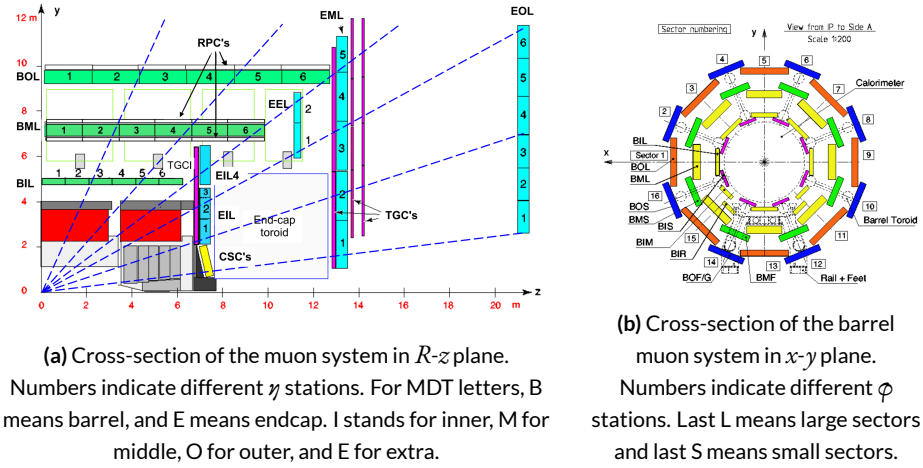

(a) Cross-section of the muon system in R-z plane. Numbers indicate different η stations. For MDT letters, B means barrel, and E means endcap. I stands for inner, M for middle, O for outer, and E for extra.

(b) Cross-section of the barrel muon system in x-y plane. Numbers indicate different φ stations. Last L means large sectors and last S means small sectors.

Figure 2.4: The overall layout of the ATLAS MuonSpectrometer.

The muon spectrometer (Figure 2.4) surrounds the calorimeters and includes three large superconducting air-core toroids. The field integral of the toroids ranges between 2 and 6 T/m for most of the detector. Because of this bending power, the MS measures Muon momentum stand-alone, with $\sigma_{p_T}/p_T \sim 10\%$ at $p_T = 1$TeV. Muon Drift Tubes (MDT) and Cathode Strip Chambers (CSC) provide precision tracking. Each MDT has 80 μm spacial resolution, with an alignment precision of 30 μm. Resistive Plate Chambers (RPC) in the barrel and Thin Gap Chambers (TGC) provide

triggering, with 1.5-5 ns timing resolution. The muon spectrometer defines the overall dimensions of the ATLAS detector.

2.2.5 Trigger and Data Aquasition

A dedicated trigger system is used to select events[36]. The first-level trigger (L1) is implemented in hardware and uses the calorimeter and muon detectors to seed regions of interest (RoI) and reduce the accepted event rate to 100 kHZ. This is followed by a software-based high-level trigger (HLT) that reduces the accepted event rate to 1 kHZ on average. To avoid too high accept rates for certain triggers, the triggers are often prescaled, which means the accepted events get rejected at the prescale. For example, a prescale of two means only every second event passing all trigger conditions gets accepted.

Over 2015 and 2016, both the LHC and the ATLAS performed outstandingly [37]. The total data recording efficiency for ATLAS is around 92%.

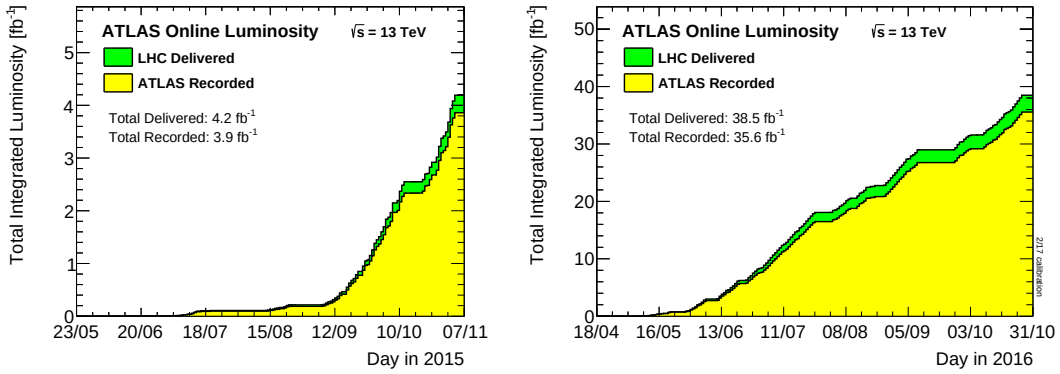

(a) 2015 **(b)** 2016

Figure 2.5: Cumulative luminosity versus time delivered to (green) and recorded by ATLAS (yellow) during stable beams for pp collisions at 13 TeV centre-of-mass energy.

Ugliness is in a way superior to beauty because it lasts.

Serge Gainsbourg

3

Data and Simulation

4

Conclusion

Di-Higgs search has a short history, but will have a long future. This thesis presents a search for both resonant and non-resonant production of pairs of Standard Model Higgs bosons has been carried out in the dominant $b\bar{b}b\bar{b}$ channel, using 27.5–36.1 fb^{-1} of LHC pp collision data at $\sqrt{s} = 13$ TeV collected by ATLAS in 2015 and 2016. The search sensitivity of this analysis exceeds that of the previous analysis of the $\sqrt{s} = 13$ TeV 2015 dataset[3] for non-resonant signal and also across the entire mass range of 260-3000 GeV for the resonance search, with significantly improvement in the high mass resonance sensitivities. The resolved analysis has each $h \to b\bar{b}$ reconstructed as two separate b-tagged jets, and the boosted analysis has each $h \to b\bar{b}$ reconstructed as a single large-radius jet associated with at least one small-radius b-tagged track-jet. The estimated background consists mainly of multi-jet and $t\bar{t}$ events.

No significant excess is observed in the data. The largest deviation from the background-only hypothesis is observed for narrow signal models at a mass of 280 GeV in the resolved analysis, with a global significance of 2.3σ. This excess could be a trigger-turn on combined with kinematic selection effect and might not last with more data. Upper limits on the production cross section times branching ratio to the $b\bar{b}b\bar{b}$ final state are set for a narrow-width scalar and for spin-2 resonances. The 95% CL upper limit on the non-resonant production is 147 fb, which corresponds to 13.0 times the SM expectation.

Future improvement with the rest of $\sqrt{s} = 13$ TeV Run II could come from improving b-tagging, especially in the high p_{T}region. Advanced trigger technologies and selections will increase the data rate, and better jet energy and mass resolution will increase the purity in selection. With the larger dataset and improvements in physics performance, it is possible to reach twice as the current sensitivity of resonance searches. For non-resonance searches, an order of 10 times the SM expectation is more sensible at the end of Run II.

For longer term perspectives, di-Higgs measurements will continue to be one of the most important analysis that help constraining our understanding of physics beyond the Standard Model. Given the current status, it is possible that in fifteen to twenty years there will be no new discovery, and the experiments at the LHC will be able to constrain the Higgs self-coupling within unity.

As humans, we have a limited life. However, physics, as well as the understanding of the universe, is an endless journey. I sincerely hope that my biased prediction of the future of Higgs physics will be wrong, but nevertheless I am deeply honored to be a small part of this odyssey towards Veritas.

References

[1] C. Patrignani et al. Review of Particle Physics. *Chin. Phys.*, C40(10):100001, 2016. doi: 10.1088/1674-1137/40/10/100001.

[2] W.J. Stirling. 7/8 and 13/8 TeV LHC luminosity ratios. 2013. URL http://www.hep.ph.ic.ac.uk/~wstirlin/plots/lhclumi7813_2013_v0.pdf.

[3] Lyndon Evans. The Large Hadron Collider. *Annual Review of Nuclear and Particle Science*, 61(1):435–466, 2011. doi: 10.1146/annurev-nucl-102010-130438.

[4] Kaustubh Agashe, Hooman Davoudiasl, Gilad Perez, and Amarjit Soni. Warped gravitons at the CERN LHC and beyond. *Phys. Rev. D*, 76:036006, 2007. doi: 10.1103/PhysRevD.76.036006.

[5] Liam Fitzpatrick, Jared Kaplan, Lisa Randall, and Lian-Tao Wang. Searching for the Kaluza-Klein graviton in bulk RS models. *JHEP*, 09:013, 2007. doi: 10.1088/1126-6708/2007/09/013.

[6] T. D. Lee. A theory of spontaneous t violation. *Phys. Rev. D*, 8:1226–1239, Aug 1973. doi: 10.1103/PhysRevD.8.1226.

[7] G.C. Branco et al. Theory and phenomenology of two-Higgs-doublet models. *Phys. Rept.*, 516:1, 2012. doi: 10.1016/j.physrep.2012.02.002.

[8] Graham D. Kribs and Adam Martin. Enhanced di-higgs production through light colored scalars. *Phys. Rev. D*, 86:095023, 2012. doi: 10.1103/PhysRevD.86.095023.

[9] R. Gröber and M. Mühlleitner. Composite Higgs boson pair production at the LHC. *JHEP*, 06:020, 2011. doi: 10.1007/JHEP06(2011)020.

[10] Roberto Contino et al. Anomalous couplings in double Higgs production. *JHEP*, 08:154, 2012. doi: 10.1007/JHEP08(2012)154.

[11] ATLAS Collaboration. Search for pair production of Higgs bosons in the $b\bar{b}b\bar{b}$ final state using proton–proton collisions at $\sqrt{s} = 13$ TeV with the ATLAS detector. *Phys. Rev. D*, 94:052002, 2016. doi: 10.1103/PhysRevD.94.052002.

[12] ATLAS Collaboration. Search for Higgs boson pair production in the $b\bar{b}b\bar{b}$ final state from pp collisions at $\sqrt{s} = 8$ TeV with the ATLAS detector. *Eur. Phys. J. C*, 75:412, 2015. doi: 10.1140/epjc/s10052-015-3628-x.

[13] ATLAS Collaboration. Search for Higgs Boson Pair Production in the $\gamma\gamma b\bar{b}$ Final State Using *pp* Collision Data at $\sqrt{s} = 8$ TeV from the ATLAS Detector. *Phys. Rev. Lett.*, 114: 081802, 2015. doi: 10.1103/PhysRevLett.114.081802.

[14] David Griffiths. *Introduction to elementary particles*. 2008.

[15] Christopher G. Tully. *Elementary particle physics in a nutshell*. 2011.

[16] Matthew D. Schwartz. *Quantum Field Theory and the Standard Model*. Cambridge University Press, 2014. ISBN 1107034736, 9781107034730.

[17] ATLAS Collaboration. Observation of a new particle in the search for the Standard Model Higgs boson with the ATLAS detector at the LHC. *Phys. Lett. B*, 716:1, 2012. doi: 10.1016/j.physletb.2012.08.020.

[18] CMS Collaboration. Observation of a new boson at a mass of 125 GeV with the CMS experiment at the LHC. *Phys. Lett. B*, 716:30, 2012. doi: 10.1016/j.physletb.2012.08.021.

[19] R. Frederix, S. Frixione, V. Hirschi, F. Maltoni, O. Mattelaer, P. Torrielli, E. Vryonidou, and M. Zaro. Higgs pair production at the LHC with NLO and parton-shower effects. *Phys. Lett.*, B732:142–149, 2014. doi: 10.1016/j.physletb.2014.03.026.

[20] D. de Florian et al. Handbook of LHC Higgs Cross Sections: 4. Deciphering the Nature of the Higgs Sector. 2016. doi: 10.23731/CYRM-2017-002.

[21] Graham D. Kribs, Andreas Maier, Heidi Rzehak, Michael Spannowsky, and Philip Waite. Electroweak oblique parameters as a probe of the trilinear Higgs boson self-interaction. *Phys. Rev.*, D95(9):093004, 2017. doi: 10.1103/PhysRevD.95.093004.

[22] Viviana Cavaliere and Gabriel Facini. Summary of Limits on BSM Models from Diboson Searches. Technical Report ATL-COM-PHYS-2016-1071, CERN, Geneva, Sep 2016. URL https://cds.cern.ch/record/2203605.

[23] Georges Aad et al. Searches for Higgs boson pair production in the $hh \to bb\tau\tau, \gamma\gamma WW^*, \gamma\gamma bb, bbbb$ channels with the ATLAS detector. *Phys. Rev.*, D92:092004, 2015. doi: 10.1103/PhysRevD.92.092004.

[24] Lyndon R Evans and Philip Bryant. LHC Machine. *J. Instrum.*, 3:S08001. 164 p, 2008. URL https://cds.cern.ch/record/1129806. This report is an abridged version of the LHC Design Report (CERN-2004-003).

[25] ATLAS Collaboration. The ATLAS experiment at the CERN Large Hadron Collider. *JINST*, 3:S08003, 2008. doi: 10.1088/1748-0221/3/08/S08003.

[26] CMS Collaboration. The CMS experiment at the CERN LHC. *Journal of Instrumentation*, 3 (08):S08004, 2008. URL http://stacks.iop.org/1748-0221/3/i=08/a=S08004.

[27] LHCb Collaoration. The LHCb Detector at the LHC. *JINST*, 3:S08005, 2008. doi: 10.1088/1748-0221/3/08/S08005.

[28] ALICE Collaboration. The ALICE experiment at the CERN LHC. *Journal of Instrumentation*, 3(08):S08002, 2008. URL http://stacks.iop.org/1748-0221/3/i=08/a=S08002.

[29] ATLAS Collaboration. Luminosity Determination in pp Collisions at $\sqrt{s} = 7$ TeV Using the ATLAS Detector at the LHC. *Eur. Phys. J.*, C 71:1630, 2011. doi: 10.1140/epjc/s10052-011-1630-5.

[30] Paul Collier for the LHC team. LHC Machine Status. CERN Resource Review Board, 2015. URL https://cds.cern.ch/record/2063924/files/CERN-RRB-2015-119.PDF.

[31] Giulia Papotti for the LHC team. LHC Machine Status Report. CERN Resource Review Board, 2016. URL https://indico.cern.ch/event/563488/contributions/2277292/attachments/1340292/2019570/20160921_LHCC.pdf.

[32] ATLAS Collaboration. The ATLAS Experiment at the CERN Large Hadron Collider. *JINST*, 3:S08003, 2008. doi: 10.1088/1748-0221/3/08/S08003.

[33] ATLAS Collaboration. ATLAS Insertable B-Layer Technical Design Report. CERN-LHCC-2010-013. ATLAS-TDR-19, Sep 2010. URL https://cds.cern.ch/record/1291633.

[34] ATLAS Collaboration. Expected performance of the ATLAS b-tagging algorithms in Run-2. ATL-PHYS-PUB-2015-022, 2015. URL https://cds.cern.ch/record/2037697.

[35] Morad Aaboud et al. Study of the material of the ATLAS inner detector for Run 2 of the LHC. *JINST*, 12(12):P12009, 2017. doi: 10.1088/1748-0221/12/12/P12009.

[36] ATLAS Collaboration. Performance of the ATLAS Trigger System in 2015. *Eur. Phys. J. C*, 77:317, 2017. doi: 10.1140/epjc/s10052-017-4852-3.

[37] ATLAS Collaboration. ATLAS Luminosity Public Results, Run 2. 2015. URL https://twiki.cern.ch/twiki/bin/view/AtlasPublic/LuminosityPublicResultsRun2.